J MATER SCI 41 (2006) 2915–2927

Influence of physico-structural properties on the photocatalytic activity of sol-gel derived TiO_2 thin films

M. FALLET, S. PERMPOON, J. L. DESCHANVRES, M. LANGLET*
LMGP/ENSPG, BP 46, Domaine Universitaire 38402 Saint Martin d'Hères, France
E-mail: Michel.Langlet@inpg.fr

Published online: 17 March 2006

Sol-gel TiO_2 films were deposited from various sols and heat-treated at different temperatures. Fourier transform infrared spectroscopy, ellipsometry, X-ray diffraction, and scanning electron microscopy methods have been used to study physico-structural properties of the films. These properties are discussed with respect to the experimental parameters. It is shown that, depending on sol formulations and annealing temperatures, a large range of crystallite size, crystallization degree, film porosity, and surface morphology can be covered. The photocatalytic properties of the films have been studied in relation to their physico-structural properties through the photodecomposition of malic acid. This study shows that the photocatalytic activity undergoes a complex dependence on the physico-structural properties.

1. Introduction

It is well established that particle size is one of the most important parameters to be optimized for improving the catalytic or photocatalytic properties of a semiconductor. Since TiO_2 in its anatase polymorphic form is considered as the most promising candidate for photocatalytic applications, numerous articles have been devoted to size effects on the photocatalytic properties of anatase particles. Reported observations appear to be rather conflicting. Anpo *et al*. mentioned an enhanced photocatalytic activity for the hydrogenation of CH_3CCH with H_2O, which was attributed to quantization effects in nano-scale TiO_2 particles (5.5 nm diameter) [1]. Choi *et al*. also reported on the photooxidation of $CHCl_3$ and the photoreduction of CCl_4 by quantized TiO_2 particles (2–4 nm diameter) [2]. It is known that in nano-particles, quantization effects promote discrete states in the conduction and valence bands and an increase of the effective band gap, which in turn favors an enhanced photoredox potential allowing photoinduced oxydo-reduction reactions that cannot occur in bulk materials [3]. Such very small particles also impact photocatalytic properties by increasing the number of active surface sites in contact with matter to be photocatalytically decomposed and by minimizing the risks of charge carrier (electron e^- and holes p^+) recombination within the particle volume. However, the greater band gap of quantized particles reduces the absorption efficiency of near-UV radiation that usually promotes the photogeneration of charge carriers in anatase particles. Besides, very small particles favor an enhanced e^-/p^+ surface recombination rate, which offsets the benefits of ultrahigh surface area. Accordingly, several authors reported that the photocatalytic activity did not monotonically increase with decreasing size. Zhang *et al*. reported an optimal TiO_2 crystallite size of 11 nm for the photocatalytic degradation of $CHCl_3$ [4], while an optimum photooxidation of trichloroethylene was observed by Maira *et al*. in the case of 7 nm TiO_2 particles [5]. Such particle sizes appeared to be ideal compromises for minimization of surface and volume recombination rates. On the other hand, some other authors showed that the photodegradation rates of formic acid and phenol continuously increased when increasing crystallite sizes up to 15 nm [6] and 26 nm [7], respectively.

Two features can account for this great variety of results. First of all, photocatalytic characterizations are performed using very different methods (nature of the model molecule to be decomposed, oxidative or reductive decomposition procedures, gas or liquid phase decomposition), which reduces possibilities of making

*Author to whom all correspondence should be addressed.

0022-2461
DOI: 10.1007/s10853-006-5077-2

objective comparisons. On the other hand, photocatalysts are prepared using very different synthesis routes, which can specifically influence size effects. Cho *et al*. showed that the photocatalytic activity of TiO_2 particles underwent very complex dependence on the crystallite size, which was related to the choice of the crystallization methods, i.e. thermal calcination, hydrothermal treatment, or combination of both methods [8]. Besides, several authors have mentioned that crystallite size effects can hardly be decoupled from the influence of other physico-structural parameters that also depend on synthesis methods. Such physico-structural parameters include crystallization degree, crystal shape, surface area, as well as the eventual presence of a secondary, and poorly active, rutile phase [6–8]. In particular, during the preparation of anatase crystallites, agglomeration mechanisms are difficult to avoid, which cause the formation of aggregates of various sizes that also depend on the synthesis routes. Size and morphology of aggregates are additional parameters that can considerably influence mechanisms governing photocatalytic properties, i.e. intra- and inter-aggregate transfer of charge carriers and their surface recombination with reactant to be photocatalytically decomposed. Aggregates can also influence light absorption and light scattering mechanisms that determine the degree of photon interaction with photocatalytic particles. Accordingly, several authors mentioned the complex and interactive influence of crystal and aggregate sizes on the photocatalytic properties of titanium oxide [5, 7, 8]. Owing to this very complex situation, studies on the influence of crystal size, and more generally of physico-structural properties, are still a matter of primary interest in the field of TiO_2 photocatalysts.

Up to now, the influence of physico-structural properties has essentially been studied on TiO_2 particles intended for unsupported powder photocatalyst or ceramic photocatalyst applications, e.g. decontamination, purification, or deodorization of air and wastewater. Photocatalytic thin films deposited on rigid supports constitute another approach that has been often proposed. First of all, this approach can provide more convenient ways of water depollution or purification by suppressing the need of a post-separation of the photocatalyst from the photopurified water, which is unavoidable in the case of unsupported catalysts [9, 10]. Besides, photocatalytic TiO_2 films have broadened the field of photocatalysis to new applications such as (already commercialized) self-cleaning supports [11]. However, studies devoted to the photocatalytic activity dependence on the physico-structural properties of TiO_2 films have rarely been undertaken. Furthermore, compared to powdered photocatalysts, additional parameters have to be taken into account in the case of thin films. In particular, in the case where deeper layers of a film are able to participate to the photocatalytic reaction, the film thickness becomes an essential parameter to be studied and controlled. Two mechanisms can account for the participation of deeper layers to the photoreaction: (i) diffusion of the gaseous or liquid reactant to be decomposed through the pores of the film, or (ii) intergranular transfer of charge carriers and migration toward the surface in contact with reactant [12]. In both cases, thickness effects are likely to be influenced by the film porosity, another essential parameter that will influence photocatalytic properties.

In this paper, we present first studies performed in our group concerning the influence of physico-structural properties on the photocatalytic activity of sol-gel derived TiO_2 films. Films deposited from various sols were heat-treated at temperatures up to 800°C. Film thickness and porosity, crystallization degree, crystal and aggregate sizes, are first described and discussed with respect to sol formulations and heat-treatment conditions. Influence of these parameters on the photocatalytic activity of the films is then investigated.

2. Experimental

TiO_2 films were deposited from various sols. A mother sol (MS) was prepared from TIPT (tetraisopropyl orthotitanate from Fluka) diluted in absolute ethanol with a TIPT concentration $C_{TIPT} = 0.4$ mol/l, a pH of 1.27, and a water to TIPT molar ratio $r_w = 0.8$. Crystalline suspensions (CS) of TiO_2 nanoparticles were prepared from this mother solution following a multi-step procedure, which has been detailed in a previous paper [12]. The r_w ratio was first adjusted at different values by adding deionized water to the mother solution, in order to obtain a r_w value between 10 and 200. Partial dilution in water was expected to promote a slight pH increase from 1.3 to 1.6, depending on the final r_w value. The so-obtained aqueous solution was then heat-treated for 6 h in a stainless steel autoclave placed in a tubular furnace. Autoclaving temperatures ranging from 100 to 200°C were studied. Thermal regulation was achieved using a thermocouple inserted in the wall of the autoclave. This thermal treatment yielded a viscous paste constituted of agglomerated anatase particles. After thermal treatment, an exchange procedure with ethanol was performed in order to remove water from the sols, which were then ultrasonicated to achieve optimum particle dispersion. We previously showed that so-obtained crystalline suspensions in ethanol were compatible with the deposition of optical quality films [12]. Accordingly, all suspensions mentioned in the present article yielded films that, once deposited on mineral glass plates, exhibited maximal transmission losses of 0.5% in the [500–1100 nm] spectra range (not illustrated here). Transmission losses gradually increased below 500 nm and strong band edge absorption was observed below 400 nm.

In this work, films were deposited from MS and CS sols by spin-coating (20 μl; 6000 rpm) on Si (100) wafers of identical size (3.3 × 3.3 cm^2). Hereafter, the film nomenclature corresponds to the sol formulation, i.e. MS films or CS/r_w/T films (for instance CS/90/130 for a film deposited from a crystalline suspension autoclaved at

130°C with a r_w ratio of 90). Ellipsometric measurements showed that, for all the films, 90% of the substrate surface was coated with a thickness uniformity of about 1%. The other 10% corresponded to unavoidable edge effects, where the thickness was greater than in the homogenously coated area. In this study, thickness values correspond to those measured in the homogeneous area. The films were then studied without subsequent heat-treatment, or after annealing in air for 2 h at temperatures ranging from 110 to 800°C. Films up to 540 nm in thickness were studied. For that purpose, the film thickness was adjusted using a multilayer deposition procedure, i.e. the repetition of deposition/heating cycles. The intermediate heat-treatment used during the multilayer deposition procedure of CS films was performed at 110°C for 3 min in air. This treatment yielded an efficient evaporation of the liquid, i.e. ethanol (essentially) and traces of water remaining in the sol after the exchange procedure, before deposition of a subsequent layer. For MS films annealed at 500°C or more, the intermediate heat-treatment was performed at 500°C for 3 min to achieve film densification and elimination of residual alkoxy and hydroxyl groups. For other MS films (annealed at 400°C or less) the intermediate densification was performed at the temperature used for the final annealing treatment. The film thickness was observed to linearly increase with the number of single-coatings. The thickness per single-coating, measured after thermal treatment, varied from 25 to 60 nm, depending on sol formulations and annealing temperatures.

The films were characterized in transmission by Fourier transform infrared (FTIR) spectroscopy using a Bio-Rad FTS-165 spectrometer. Spectra of 300 scans were recorded in a (4000–250 cm^{-1}) range with a resolution of 4 cm^{-1}. They were analyzed after subtracting the bare Si substrate spectrum. X-ray diffraction (XRD) characterizations were performed using a Siemens D5000 diffractometer with Cu Kα_1 radiation ($\lambda = 1.54056$ Å). The diffracted intensity was recorded in a $[22 - 60°]2\theta$ range with a step of 0.02° and an integration time of 22 s. Film thickness and refractive index were measured using a Sentech ellipsometer at 632 nm wavelength. The volume porosity was estimated from the refractive index value using the Lorentz-Lorenz relationship [13]. A Philips XL 30 scanning electron microscope (SEM) was used to study film surface morphologies.

The photocatalytic activity was measured at room temperature. Titania films deposited on Si wafers were settled in a Pyrex photoreactor opened to air containing malic (2-hydroxybutanedioic) acid aqueous solution (30 ml; 3.7 10^{-4} M; natural neutral pH). Constant agitation of the solution was insured using a magnetic stirrer. Before UV-irradiation, the solution was first stirred in the dark for 60 min to reach equilibrated adsorption of malic acid at the film surface. The film was then exposed for 3 h to UV-irradiation provided by a Philips HPK 125 UV-lamp (40 mW/cm^2) using a Corning 0.52 filter ($\lambda > 340$ nm). To avoid heating of the solution during irradiation, light was passed through a circulating-water cuvette located between the photoreactor and the lamp. Small solution aliquots were periodically withdrawn in order to measure the concentration variations of malic acid as a function of time. Malic acid analysis was performed by liquid chromatography (HPLC) using a Waters 600 chromatograph, equipped with a SARASEP CAR-H column (eluent: H_2SO_4, 5×10^{-3} M; flow rate: 0.7 ml/min; detection at $\lambda = 210$ nm). The photocatalytic activity was determined from the rate of disappearance of malic acid. This acid has been chosen as a model molecule of carboxylic acids, which are the best representatives for the main constituents of intermediate products in oxidative degradation processes [14].

3. Results and discussion

3.1. FTIR characterizations

In previous works, we have shown that FTIR spectroscopy is a precious tool that provides important information not only on the chemical state of the film but also on its crystallization degree, even in the case of nano-crystalline thin films for which XRD sensitivity is rather limited [12, 15]. Fig. 1 shows FTIR spectra in the [1000–250 cm^{-1}] range for films without heat-treatment deposited from various sols. The MS film (Fig. 1a) exhibits typical spectrum of an amorphous oxo-polymer, i.e. an amorphous oxide network with unreacted alkoxy (OR) and hydroxyl (OH) chain-end groups [16]. The signature of OR and OH groups was also observed in the [4000–1000 cm^{-1}] spectral region (not illustrated here). For CS films, traces of water but no alkoxy groups could be detected by FTIR. CS films exhibit two major absorption bands around 430 and 300 cm^{-1} (Fig. 1b–d), which roughly correspond to transversal optical (TO) modes of anatase [17]. Intensity and width of TO absorption bands are closely related to the structural ordering (dispersion of the Ti–O–Ti bridging bond angles and interatomic distances). For amorphous films, broad TO modes overlap and constitute a single broad band around 400 cm^{-1}. As crystallization takes place, they increase in intensity and sharpen, thus forming two separate bands. Resolved bands observed in

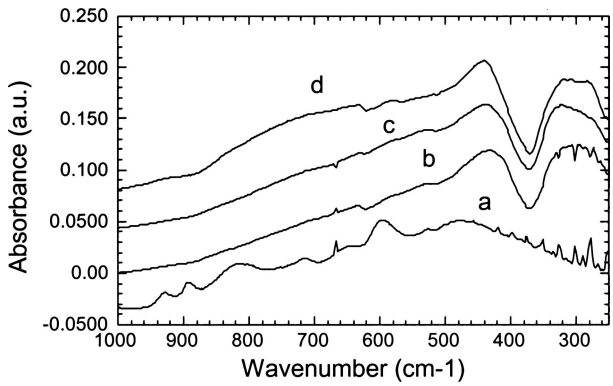

Figure 1 FTIR spectra of as-deposited (a) MS, (b) CS/200/100, (c) CS/130/90, and (d) CS/10/200 films.

Fig. 1b–d indicate that wellcrystallized CS films were deposited at room temperature. However, some small variations can be observed on the spectra of these films. In particular, for the CS/10/200 film a pronounced and broad shoulder appears on the high wavenumber side of the 430 cm^{-1} band between 900 and 500 cm^{-1} (Fig. 1d), which is less marked for CS/90/130 (Fig. 1c) and CS/200/100 films (Fig. 1b). It is known that IR spectra of titanium oxide are very sensitive to light scattering induced by the grain size and/or sample porosity [18, 19]. IR light scattering is promoted by multiple reflections induced by the refractive index difference at the grain/pore interface. This diffusion mechanism yields IR spectra showing complex combinations of multiple LO/TO vibration modes. For more diffusive films, LO modes appear more markedly and LO/TO splitting causes broadening of absorption bands toward higher wavenumbers. The high wavenumber shoulder observed in Fig. 1d suggests that a CS/10/200 film provokes more IR light scattering than other CS films, which would indicate a greater porosity and/or grain size than for films autoclaved with a greater r_w or at lower temperature.

Fig. 2 shows FTIR spectra of MS and CS/90/130 films heat-treated at temperatures up to 400°C. All MS films heat-treated between 110 and 350°C exhibited a similar spectrum, which typically corresponded to that of an amorphous TiO_2 film (Fig. 2a). No alkoxy groups could be evidenced for films heat-treated at110°C or more. The MS film heat-treated at 400°C exhibits two sharp bands located at 435 and 260 cm^{-1} (Fig. 2g), which closely match TO mode positions of anatase single crystal [17]. This indicates that MS film crystallization takes place in the (350–400°C) thermal range. CS films exhibit very different behavior (Fig. 2b–f). The previously LO-related high wavenumber shoulder gradually disappears when increasing temperature up to 400°C, while the 430 cm^{-1} TO absorption band slightly sharpens and increases in intensity. This TO band evolution suggests that the films undergo a progressive crystallization. On the other hand, gradual disappearance of the LO shoulder suggests that optical diffusion, which promotes LO mode excitation, progressively decreases, i.e. the films undergo a gradual densification mechanism. Besides, the broad band around 300 cm^{-1} follows a progressive shift from 330 to 265 cm^{-1} together with a slight intensity increase. The 265 cm^{-1} wavenumber position is very close to that of the second TO mode of anatase, which suggests that the initial broad band would be constituted of a LO component at 330 cm^{-1} and a TO component at 265 cm^{-1}. Thus, the thermally induced shift of this band can presumably be also attributed to a progressive film densification, which promotes LO mode disappearance to the benefit of TO modes. Films deposited from other CS sols exhibited FTIR spectrum evolutions similar to that of CS/90/130 films.

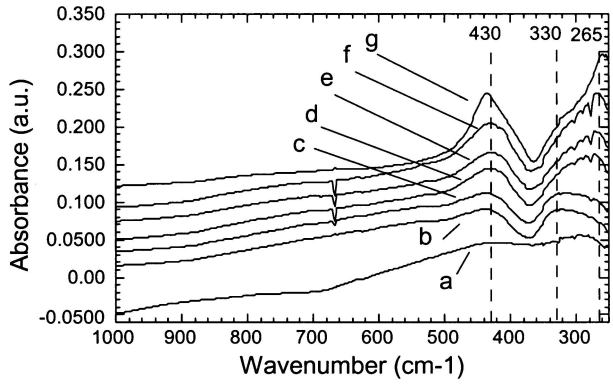

Figure 2 FTIR spectra of MS films annealed at (a) 350°C, and (g) 400°C, and CS/90/130 films (b) not annealed, or annealed at (c) 110°C, (d) 200°C, (e) 300°C, and (f) 400°C.

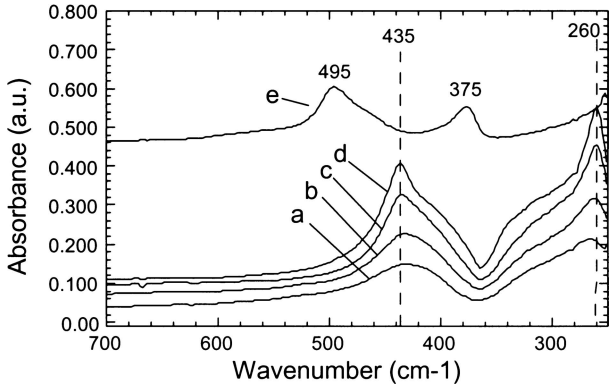

Figure 3 FTIR spectra of CS/90/130 films annealed at (a) 400°C, (b) 500°C, (c) 600°C, (d) 700°C, and (e) 800°C.

Fig. 3 shows FTIR spectra of CS/90/130 films annealed between 400 and 800°C. Compared to what happens below 400°C, TO bands undergo very pronounced growth with increasing temperature up to 700°C and noticeably sharpen (Fig. 3a–d). This feature indicates a thermally induced structural ordering, i.e. an increase of the film crystallization degree. Both bands also experience a slight shift toward 435 and 260 cm^{-1}, i.e. wavenumber positions reported for anatase single crystal. While the TO band at 260 cm^{-1} grows and sharpens, the LO component at 330 cm^{-1} progressively vanishes and appears reduced to a weak shoulder after annealing at 700°C (Fig. 3d). According to previous considerations, this LO/TO modification would indicate that films annealed in the [400 – 700°C] range undergo a marked thermally activated densification. The 435 cm^{-1} TO band follows a similar trend, i.e. the band grows and sharpens, which yields the appearance of a small shoulder located around 390 cm^{-1}. This latter probably corresponds to another LO mode of anatase. Let us note that 330 and 390 cm^{-1} positions do not strictly correspond to LO modes reported for anatase single crystal [17].

However, it has previously been shown that, owing to the high dielectric constant of titanium oxide, LO/TO splitting can be strongly affected by crystal shapes and aggregation states [20], which would explain differences observed in the FTIR spectra of single crystals and polycrystalline films. Weak LO shoulders observed in Fig. 3d suggest that films annealed at 700°C are still slightly porous. Accordingly, the spectrum of Fig. 3d agrees fairly

well with the spectrum of a semi-dense anatase film reported by other authors [21]. Let us note that films annealed at 800°C (Fig. 3e) exhibit absorption bands of a pure rutile phase [20], while such bands cannot be observed in the spectrum of films annealed at 700°C. This indicates that anatase/rutile phase transformation rapidly occurs between 700 and 800°C. Finally, it has to be mentioned that, in the (400 − 800°C) thermal range, all MS and CS films followed FTIR spectrum variations similar to that observed for CS/90/130 films.

To summarize, results illustrated in Figs 2–3 suggest that broad bands, initially observed around 430 and 300 cm^{-1}, are combinations of TO and LO modes, and that thermally induced shifts and shape modifications of these bands result from densification and crystallization features that seem to follow a bi-regime mechanism. Below 400°C, crystalline CS films undergo slight densification and crystallization effects, while crystallization of MS films takes place between 350 and 400°C. Above 400°C, both CS and MS films undergo pronounced densification together with marked structural modifications. Such effects have been clarified by means of ellipsometry and XRD measurements.

3.2. Ellipsometric characterizations

Figs 4–5 show refractive index and thickness variations of 7-layer films, deposited from different MS and CS sols and heat-treated at various temperatures. For MS films, only crystalline films were studied, i.e. films annealed at 400°C or more. All films undergo a progressive thickness (refractive index) decrease (increase) with increasing temperature, which suggests a thermally activated film densification. For CS films, densification appears weakly marked for temperatures up to 400°C, which would indicate that slight densification effects illustrated by FTIR spectra remain below or very close to the ellipsometric measurement sensitivity. A thermally activated densification is clearly evidenced at higher temperatures, which supports the bi-regime behavior illustrated by FTIR spectra. Besides, for a same number of deposited single-layers,

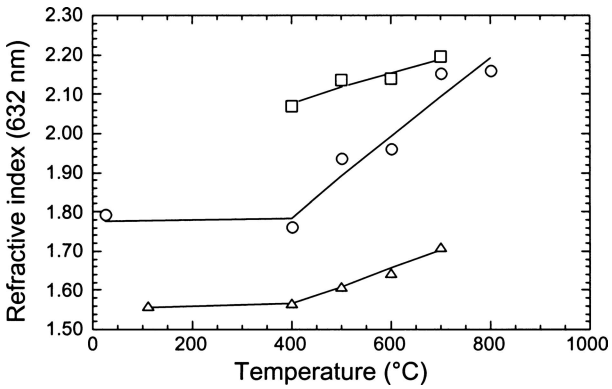

Figure 4 Refractive index measured at 632 nm versus annealing temperature for MS (□) , CS/10/200 (Δ), and CS/90/130 films (O).

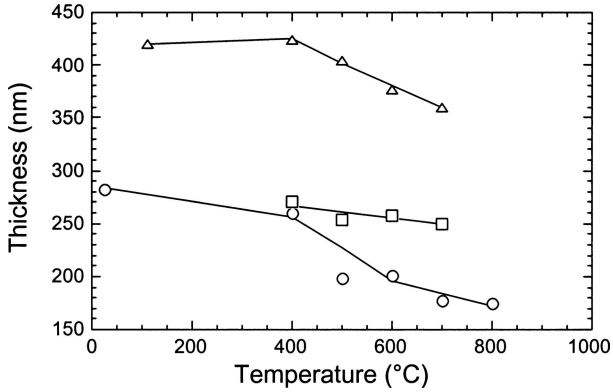

Figure 5 Variations of thickness with annealing temperature for MS (□), CS/10/200 (Δ), and CS/90/130 films (O).

CS/10/200 films exhibit at any temperatures smaller refractive indices than CS/90/130 films, which confirms their greater volume porosity suggested by FTIR spectra of Fig. 1. On the other hand, MS crystalline films exhibit greater refractive indices than CS films, which indicates that thermal densification takes place more easily than in CS films. This behavior is related to the initially amorphous character of MS films. It is known that in the amorphous state, densification proceeds through viscous flow mechanism while atomic diffusion mechanism is involved in the case of crystalline materials, and that the former mechanism is much faster than the latter [22]. It is therefore likely that for MS films, densification efficiently takes place in the amorphous state during initial stages of heating.

It is known that, in the case of pure oxide films, the volume porosity P (in vol%) can be fairly well estimated from the refractive index value n, using the Lorentz-Lorenz relationship [13]

$$1 - P/100 = (n^2 - 1)/(N^2 - 1) \times (N^2 + 2)/(n^2 + 2) \quad (1)$$

where N corresponds to the bulk material refractive index ($N \approx 2.50$ for anatase [23]). Besides, a simple calculation shows that for a given film surface S, the film thickness t is related to the porosity by

$$St = St_0 + St \times P/100 \qquad \text{or} \qquad 1 - P/100 = t_0/t \quad (2)$$

where t_0 corresponds to an effective thickness, which accounts for the actual volume of deposited solid matter. For a given sol, the volume of deposited solid matter (i.e. the effective thickness t_0) is not expected to vary with annealing temperature provided that no thermally induced chemical or structural change occurs which would promote a modification of the titania density, e.g. anatase/rutile phase transformation. For pure anatase films, the $1–P/100$ value derived from Lorentz-Lorenz relationship should therefore linearly increase with increasing $1/t$. This feature is illustrated in Fig. 6 for anatase films of Figs 4 and 5 annealed at temperatures up to 700°C (i.e. the threshold temperature of anatase/rutile transformation). Most films

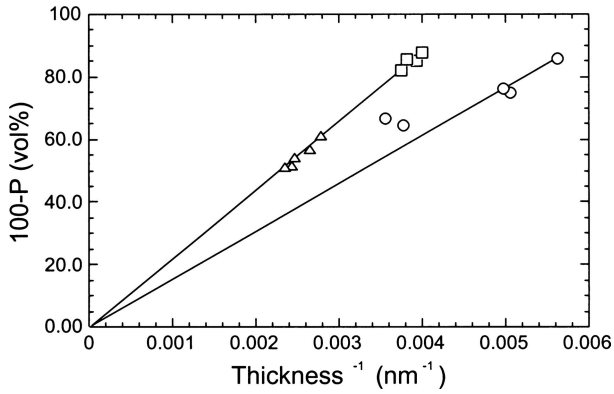

Figure 6 Thickness dependence of the volume porosity (P) for MS (□), CS/10/200 (Δ), and CS/90/130 films (O) heat-treated at various temperatures. The volume porosity was calculated from the refractive index using the Lorentz-Lorenz relationship.

follow a linear variation, which confirms that refractive index and thickness variations of Figs 4 and 5 actually illustrate densification features. The volume porosity ranges between 12 and 50% depending on sol formulations and heat-treatment temperatures. For a same number of deposited single-coatings, slopes of the straight lines, which correspond to the effective film thickness t_0, exhibit some differences. This presumably indicates variations in rheologic properties of the different sols, which would in turn modify deposition conditions and amounts of deposited solid matter per single-coating. In Fig. 6, only CS/90/130 films annealed at temperatures lower than 400°C experience some small deviations from the linear variation. A similar trend was also observed for CS/200/100 films (not illustrated here). It is possible that those films were not constituted of a pure titanium oxide. Though residual alkoxy groups could not be detected by FTIR spectrometry for crystalline films, it is possible that a small amount of such groups are still present at the grain surface for CS films annealed at low temerature. These groups might increase the refractive index value, compared to a pure oxide film of similar porosity, i.e. alkoxy groups might partially fill pores of the films, which would yield an underestimation of the porosity deduced from the Lorentz-Lorenz relationship. Nevertheless, it has been considered in the present work that the porosity value deduced from the Lorentz-Lorenz relationship provides a reliable illustration of thermally induced densification features and that the effective thickness measured for crystalline films reasonably accounts for the actual amount of deposited solid matter. Both parameters will be referred to in next sections.

3.3. XRD characterizations

Fig. 7 shows XRD patterns of CS/90/130 films annealed at various temperatures. XRD data confirm that pure anatase films without preferential orientation were obtained for annealing temperatures up to 700°C (curve b, insert of Fig. 7), while annealing at 800°C yielded pure rutile films (curve c, insert of Fig. 7). Fig. 7 indicates that the (101) anatase reflection undergoes intensity increase and width decrease with increasing annealing temperature, which illustrates an enhancement of the crystallization degree and crystallite size. All CS crystalline films exhibited similar trends. XRD data confirmed that MS films annealed at 350°C or less were amorphous. MS crystalline films annealed at 400°C or more underwent crystallization degree and crystallite size increase with increasing temperature. Besides, a temperature increase also yielded a preferential orientation of crystallites along the [001] direction (curve a, insert of Fig. 7).

The average crystallite size of MS and CS films was estimated, using Scherrer's formula, from the full width at half maximum (FWHM) of the (101) reflection of anatase (or (110) reflection of rutile) corrected from the diffractometer resolution (Fig. 8). Fig. 8 confirms FTIR data illustrated in Figs 1–3. First of all, non-annealed

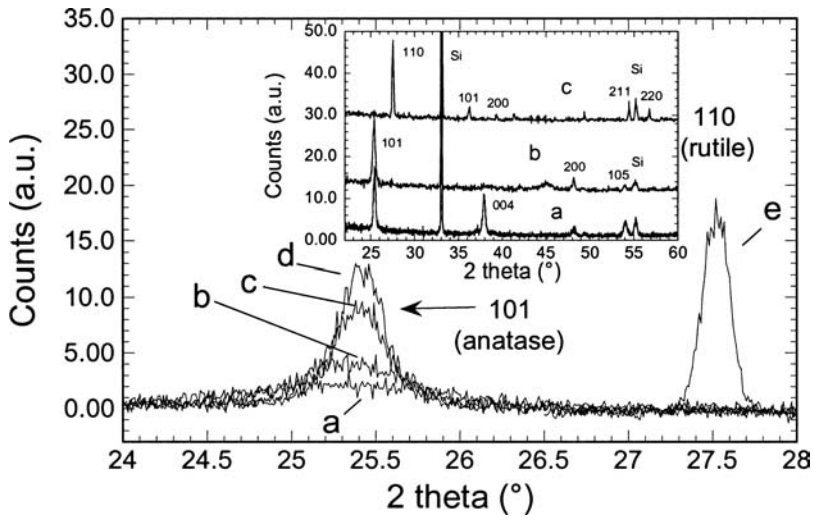

Figure 7 XRD patterns in the [24−28°] 2Θ range for CS/90/130 films annealed at (a) 400°C, (b) 500°C, (c) 600°C, (d) 700°C, and (e) 800°C. The insert shows XRD patterns in the [22 − 60°]2 Θ range for (a) a MS film annealed at 700°C and for CS/90/130 films annealed at (b)700°C and (c) 800°C.

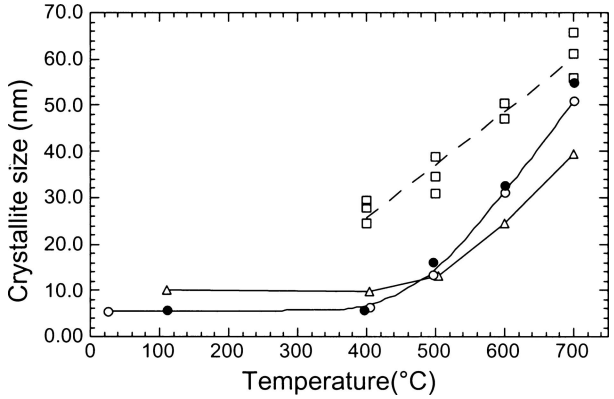

Figure 8 Variations of crystallite size with annealing temperature for MS (□), CS/10/200 (△), CS/90/130 (O), and CS/200/100 films (●).

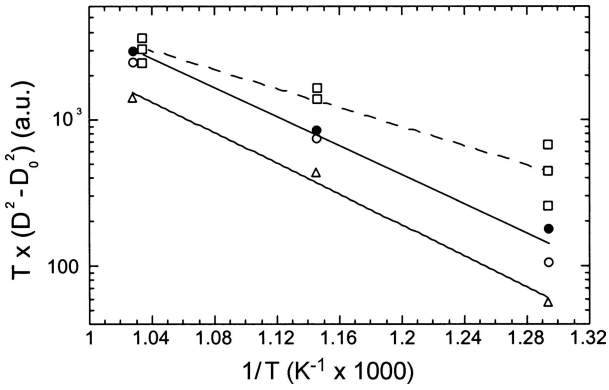

Figure 9 Arrhenius representation of the crystallite size (D) variations versus temperature T in the range [500 − 700°C] for MS (□), CS/10/200 (△), CS/90/130 films (O), and CS/200/100 films (●).D_0 corresponds to the D value measured on corresponding non-annealed films.

CS/10/200 films exhibit a greater crystallite size than CS films derived from sols autoclaved at weaker temperature and/or with a greater r_w ratio. In a previous work, we have shown that, during autoclaving, crystallization proceeds through a nucleation/growth mechanism in the liquid medium [12]. Nucleation, which promotes the homogeneous formation of smaller crystallites, is favored by a greater water amount (r_w ratio), while higher autoclaving temperatures promote growth of larger crystallites. Accordingly, in the present work CS/10/200 yielded a crystallite size around 10 nm, while sols processed at weaker temperature and/or with a greater r_w ratio yielded a crystallized size around 6 nm. Others authors showed the possibility to obtain smaller crystallites, of about 2 nm in size, from aqueous sols [2, 5]. In these works, sols were processed with a titanium precursor concentration that was much weaker than in the present study. Crystal growth relies on the interaction probability of precursor species diluted in the sol, which increases when increasing the precursor concentration. In the present work, rather concentrated sols were used in order to deposit films of consequent thickness, which would explain that the crystal size could not be decreased below a certain threshold.

Fig. 8 also confirms FTIR data showing that CS films undergo a bi-regime mechanism with increasing temperature. Below 400°C, no or very weak crystal growth could be evidenced. Above 400°C, the crystal size significantly increases with increasing temperature. A maximal size around 50 nm is measured after annealing CS/90/130 or CS/200/100 films at 700°C. Rutile films annealed at 800°C exhibited a much larger crystal size of 140 nm, showing that phase transformation proceeded together with an important crystal growth. It has to be noted that, despite a larger initial crystal size, CS/10/200 films follow a less marked crystal growth than CS films issued from sols processed at lower temperature and/or with a greater r_w ratio. All these features traduce a growth mechanism governed by atom mobility at grain boundaries. It has been shown that for such a growth mechanism, the crystal size (D) dependence on temperature T can be expressed as

$$D^2 = D_0^2 + 8m_0 st/T \times \exp(-E_a/kT) \qquad (3)$$

where D_0 corresponds to the initial grain size, t is the annealing time, s an apparent surface free energy associated to the initial configuration of the grain, m_0 a constant, and E_a an apparent activation energy [24]. For a same annealing time (2 h in our study), the term$(D^2 - D_0^2) \times T$ should therefore follow a classical Arrhenius law, when plotted as a function of $1/T$. This is illustrated in Fig. 9, whereD_0 has been considered to be the crystal size measured for non-annealed CS films. All CS films follow a linear trend, with comparable activation energy of about 100 kJ/mol. However, while for CS/90/130 and CS/200/100 films, which have a similar D_0 value of 6 nm, the crystal sizes of annealed films are very comparable, these sizes are significantly weaker for CS/10/200 films. This is because, owing to a larger D_0 value of 10 nm measured for these films, mobility at grain boundaries is weaker, i.e. the apparent surface energy s is weaker than for films with a smaller initial D_0. Fig. 9 also shows that MS films follow a different trend (in that case, the line has been plotted only to guide the eye). Because such films are initially non-crystalline, crystallization is likely to occur through a nucleation/growth mechanism within the amorphous phase [22]. In the amorphous state, atom mobility is fast and crystals rapidly grow. Accordingly, at any temperatures MS films exhibited greater crystal sizes than CS films. After annealing at 400°C, a crystal size around 25 nm has been measured, which increased up to 60 nm for films annealed at 700°C. It has also to be mentioned that for a same annealing temperature, crystal sizes were more dispersed for MS films than for CS films. This would suggest that growth at grain boundary is a better controlled process, which relies on the sol formulation, than nucleation/growth in amorphous medium.

In sol-gel derived TiO_2 oxo-polymers, residual alkoxy groups play a role of structural impurities and inhibit titanium oxide crystallization. This is the reason why sol-gel

routes developed to prepare TiO_2 crystallites in liquid suspensions were based on processing (reflux or autoclaving) of aqueous sols [12, 15, 25–30]. A great amount of water favored a complete hydrolysis of alkoxy groups and in turn promoted crystal nucleation/growth. On the other hand, titanium alkoxy groups are thermally very stable and require a temperature between 300 and 400°C to be fully thermally decomposed [31, 32]. This would explain why heating above 300–400°C is required for inducing crystallization in titanium oxo-polymers. Our results are in good agreement with such observations, showing that MS film crystallization starts at about 400°C. Thus it is inferred that, though not detected by FTIR, very small amounts of alkoxy groups are still present in MS films annealed at 350°C or less, which inhibit film crystallization. It is interesting to note that, for CS films, crystal growth starts at the temperature needed to crystallize MS films, i.e. 400°C. This observation suggests that, even in as-deposited crystalline CS films, alkoxy groups are still present, presumably at the crystal surface. Alkoxy (ethoxy) groups, though not detected either by FTIR, are all the more likely to be present in small amount, as films were deposited from crystalline suspensions in ethanol (after a water/ethanol exchange procedure). The presence of such groups at temperatures up to 400°C would in turn inhibit crystal growth at grain boundaries.

The crystallization degree of CS crystalline films annealed up to 700°C was estimated from the net area of the (101) anatase reflection. The diffracted intensity not only accounts for the crystalline fraction, i.e. the ratio of the crystallite amount to the total amount of solid matter, but also depends on the actual amount of deposited matter. Thus, an apparent crystalline fraction F_c has been defined as the (101) anatase reflection intensity normalized to t_0 the effective film thickness defined in Section 3.2. For comparison purpose, a 100% reference F_c value has been arbitrary fixed to be the crystalline fraction measured for a CS/90/130 film heat-treated at 700°C. Thus, this 100% reference value does not necessarily account for a totally crystallized film. For partially oriented crystalline MS films, F_c has been derived from the sum of the (101) and (004) reflection areas. For this new F_c definition, the CS/90/130 film heat-treated at 700°C has again been taken as a reference, in such a way that oriented MS films and non-oriented CS films could be compared on a same graph (Fig. 10). All asdeposited CS films exhibit a comparable F_c value of 60 +/− 10%, which confirms that a certain amount of amorphous matter is present in the film. Previous TEM studies showed that films deposited at room temperature from CS sols autoclaved with a sufficient water amount were constituted of well crystallized grains, and that amorphous mater was located at the crystal surface [12]. This amorphous matter presumably consists of alkoxy groups (for low annealing temperatures) and structurally non-organized Ti–O–Ti surface bonds. For MS films, the F_c value rapidly jumped from 0 to 80% when increasing temperature from 350 to 400°C. For all MS and CS crystalline films, Fig. 10 shows that F_c values increased comparatively and smoothly with crystallite size. This would indicate that crystallization and crystal growth proceed through a same mechanism, which would be governed by the fraction of amorphous matter present at the grain surface. Further TEM studies have been planed, which will allow a better understanding of the crystalline properties of MS and CS films annealed at various temperatures.

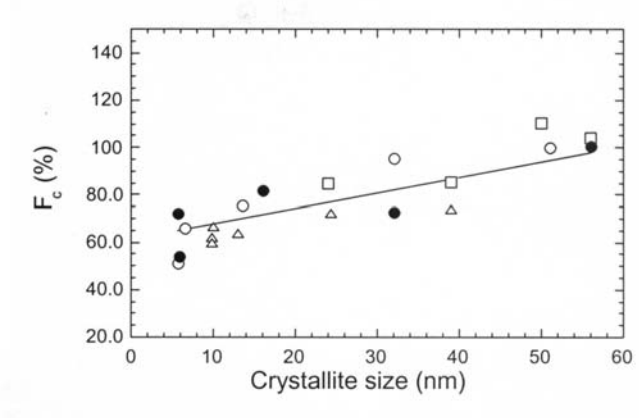

Figure 10 Normalized crystalline fraction F_c versus crystallite size for MS (□), CS/10/200 (Δ), CS/90/130 films (O), and CS/200/100 films (•) heat-treated at temperatures up to 700°C.

3.4. Electron microscope characterizations

Fig. 11 shows SEM surface images (×40000 magnification) of MS, CS/10/200, and CS/90/130 films. An MS film annealed at 700°C exhibits a very homogenous and smooth granular surface with weakly marked grain boundaries (Fig. 11a). The grain size is approximately 50 nm, which agrees rather well with crystal sizes deduced from XRD measurements. This feature suggests that grains observed in Fig. 11a correspond to nonaggregated single crystals constituting the film. No particular surface morphology could be evidenced for MS films annealed at lower temperatures because the crystal size was below the sensitivity threshold of our microscope. A non-annealed CS/10/200 film exhibits a very rough and non-uniform granular surface with marked grain boundaries (Fig. 11b). The grain size of 100–200 nm is much greater than the crystal size measured for this film (10 nm), which indicates that observed grains correspond to aggregated crystals. The large inter-aggregate porosity observed in Fig. 11b can account for the rather low refractive index measured for this film (Fig. 4). After annealing at 700°C, the CS/10/200 film exhibits similar morphology features (Fig. 11c), i.e. aggregates are still observed and present a size comparable to that observed in Fig. 11b. Nevertheless, the inter-aggregate porosity seems to be more pronounced than before heat-treatment, and aggregates appear to be finely divided into smaller grains of about 50 nm in size, which probably correspond to single crystals. CS/90/130 films partly behave similarly to CS/10/200

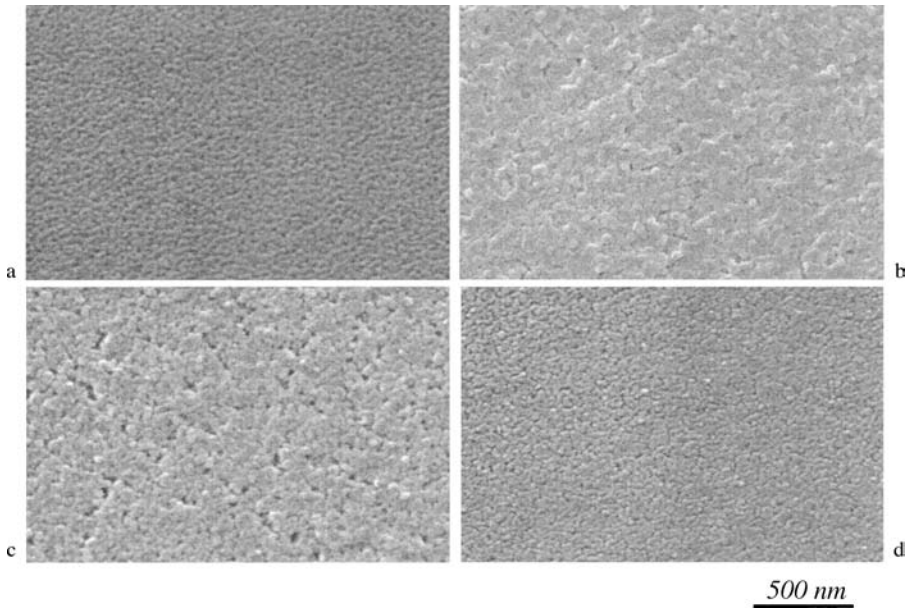

Figure 11 SEM surface images of (a) a MS film annealed at 700°C, a CS/10/200 film (b) non-annealed or (c) annealed at 700°C, and (d) a CS/90/130 film annealed at 700°C. Magnification was ×40000.

films, i.e. they exhibited an aggregated morphology and the aggregate size did not significantly vary with heat-treatment. Fig. 11d, which corresponds to a CS/90/130 film annealed at 700°C, also indicates that, compared to CS/10/200 films, CS/90/130 films are more uniform and are composed of finer aggregates (around 100 nm in size) and much smaller pores. As for CS/10/200 films, a fine texture is observed within aggregates of the CS/90/130 film annealed at 700°C, which is attributed to single crystals. All other CS films exhibited morphology features similar to those of CS/90/130 films. We previously indicated that CS sols were constituted of aggregated crystallites [12]. Light scattering measurements showed that, in CS/90/130 sols, the aggregate size was about 100 nm, and that this size increased when decreasing the water amount in the sol. This probably means that grains observed in Fig. 11b–d correspond to aggregates already present in the solution. Since CS films did not show any significant variation of the aggregate size with annealing, it is concluded that for temperatures ranging up to 700°C, no sintering process occurred that would yield aggregate growth and inter-aggregate pore reduction. This also implies that thermally activated densification features illustrated in Figs 4–6 preferentially take place within, rather than between, aggregates. Such a densification might in turn promote a slight aggregate size reduction and a more pronounced inter-aggregate porosity, which seems to be illustrated in Fig. 11b and c.

3.5. Photocatalytic characterizations

3.5.1. General features

Blank UV irradiations performed for 3 h without titania films did not allow to detect any variation of the malic acid concentration, which indicated that no photolysis occurred over the whole duration of the photocatalytic experiments. After exposing the films in the dark for 60 min the solution concentration was observed to decrease by 1 to 2 mol% indicating malic acid adsorption at the film surface. The sensitivity of our measurements did not allow any correlation between the adsorption yield and the film nature (sol formulation, film thickness, heat-treatment temperature). In the presence of the films, the malic acid photodecomposition systematically followed an apparent zero kinetic order over a period of 120 min or more, i.e. the amount of photocatalytically decomposed malic acid linearly increased with UV exposure time. This is illustrated in Fig. 12 for crystalline MS films annealed at various temperatures. Photodecomposition was observed to slow down for longer exposure duration. No film degradation could be observed after

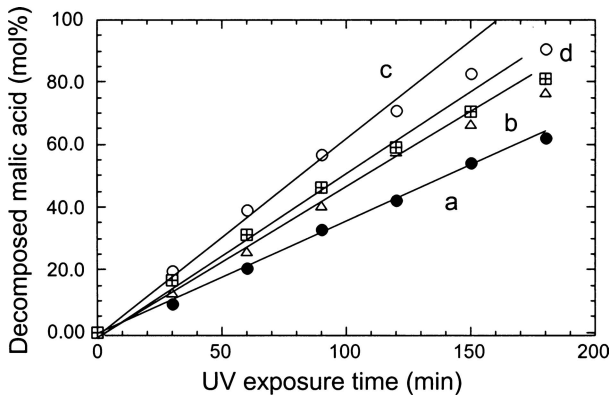

Figure 12 Molar fraction of decomposed malic acid versus UV exposure time for MS films annealed at (a) 400°C, (b) 500°C, (c) 600°C, and (d) 700°C.

photocatalysis experiments, which might explain such a feature. It is therefore likely that a decomposition threshold exists, above which the malic acid decomposition is slower. In this work, the photocatalytic activity has been defined as the mole percentage of malic acid decomposed after 120 min UV exposure.

3.5.2. Thickness dependence of the photoactivity

Fig. 13 shows variations of the photocatalytic activity as a function of thickness for as-deposited CS/30/200 and CS/90/130 films. Let us note that these films only differed in their porosity, which was determined to be 40 vol% for the former and 30 vol% for the latter. Other physico-structural properties were comparable for both films, including crystal size, aggregate size, crystalline fraction, and did not vary with film thickness. Fig. 13 shows that the photocatalytic activity gradually increases with film thickness. It means that the inner part of films participates to malic photodecomposition. However, this activity increases more slowly than the film thickness. For a true heterogeneous catalystic regime, the reaction rate is expected to be proportional to the mass of catalyst [14], i.e. the photoactivity linearly increases with film thickness. In addition, CS/90/130 films exhibit a stronger photoactivity than CS/30/200 films. Since these films only differ in their volume porosity, it is concluded that differences illustrated in Fig. 13 originate from densification effects. For a same thickness, denser films are richer in TiO_2 particles than porous ones, which might explain in part the stronger photocatalytic activity of CS/90/130 films. To take this feature into account, a relevant representation consists in plotting the photoactivity as a function of the specific thickness defined in Section 3.2, which accounts for the actual amount of deposited photocatalyst. This representation is shown in the insert of Fig. 13. It can be seen that the activity is still greater for CS/90/130 films, which suggests that porosity effects directly influence the photoactivity apart from the amount of deposited TiO_2 particles.

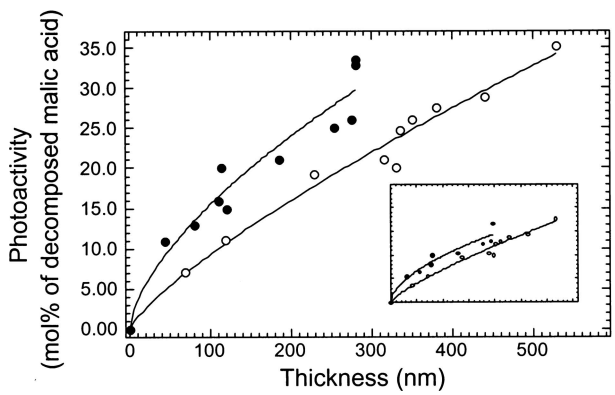

Figure 13 Photoactivity versus thickness for as-deposited CS/30/200 (O) and CS/90/130 films (•). The insert shows similar variations versus the effective film thickness t_0 defined in text.

As explained in introduction, two mechanisms can account for the participation of the inner part of the film to the photocatalytic reaction. Liquid reactant adsorbed at the film surface might be able to diffuse through the pores, inducing a greater quantity of TiO_2 particles involved in the photocatalytic reaction. In that case, the reactant diffusion should be favored by a greater porosity and, for a same effective thickness, the photoactivity of more porous films should be stronger than that of dense films. This assumption is denied by variations illustrated in Fig. 13. On the other hand, TiO_2 particles that are not directly in contact with the matter to be photocatalytically decomposed might be able to participate in the photocatalytic process, provided that an efficient transfer of charge carriers occurs between particles. A too high porosity can reduce the intergranular transfer, thus limiting the photocatalytic activity of the film, which seems to be illustrated in Fig. 13. We can thus conclude that intergranular charge transfer governs the thickness dependence of photoactivity for CS/30/200 and CS/90/130 films. In this case, the recombination of photoinduced electron-hole pairs, occurring during migration from the deeper layers toward the film surface, can in turn affect the photocatalytic activity. An increase of the recombination probability might explain the non-linear increase of photoactivity with increasing film thickness. Since intergranular transfer is hindered by the film porosity, photo-generated charge carriers are likely to accumulate at the grain boundaries, which would promote their recombination at the grain surface.

Grain size and crystalline fraction are other parameters that can influence intergranular transfer and recombination mechanisms at the surface or within the volume of TiO_2 particles. For a same porosity degree, smaller grain sizes favor a better intergranular transfer, by promoting a greater intergranular contact surface, but also enhance the predominance of surface recombination over volume recombination, owing to a smaller volume and greater surface area. On the other hand, a greater amount of amorphous matter at the crystal surface, i.e. a weaker crystalline fraction, increases the surface recombination probability by inducing more surface defects that play a role of recombination centers. To provide further insight into the respective influence of the different physico-structural parameters, the photocatalytic activity of MS, CS/10/200, and CS/90/130 films, was studied as a function of annealing temperature. Since the photocatalytic activity strongly depends on the amount of deposited photocatalyst (Fig. 13), films of rather similar effective thickness (150 to 220 nm) were studied. Furthermore, to allow a more objective comparison, photocatalytic activities were normalized with respect to the effective thickness. This normalized activity accounts, therefore, for the intrinsic activity of each active site [8], which in turn relies on surface or volume recombination probability and efficiency of the intergranular charge carrier transfer.

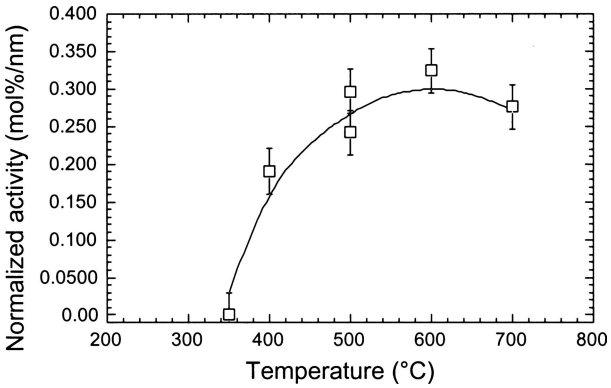

Figure 14 Normalized photoactivity versus annealing temperature for MS films. The photoactivity has been normalized with respect to the effective film thickness t_0. Lines are drawn only to guide the eye.

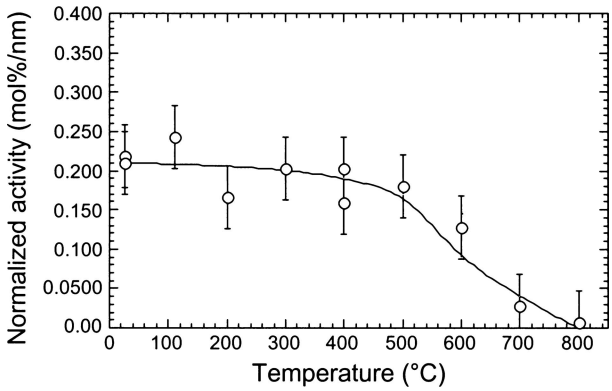

Figure 15 Normalized photoactivity versus annealing temperature for CS/90/130 films. The photoactivity has been normalized with respect to the effective film thickness t_0. Lines are drawn only to guide the eye.

3.5.3. Normalized photoactivity of MS films

Variations of the normalized photoactivity of MS films with annealing temperature are illustrated in Fig. 14. MS films annealed up to 350°C did not show any activity, which confirms that an amorphous phase yields very poor photo-generation of charge carrier and promotes fast recombination on structural defects. The photoactivity of MS films strongly increases when increasing temperature up to 600°C. It is primarily due to an increase of the film crystallization degree. It is likely that thermally activated densification of these films also favors an enhanced intergranular transfer, which in turn promotes a greater activity. Fig. 14 shows that the photoactivity reaches a maximum at about 600°C, and then seems to decrease with further temperature increase. We have previously indicated that MS films undergo a marked thermally activated crystal growth. Features illustrated in Fig. 14 suggest therefore that there exists an optimum crystal size, which would be about 50 nm for MS films annealed at 600°C (see Fig. 8). This is a rather elevated value when compared to optimum sizes reported in literature devoted to powder photocatysts. This observation confirms that, for thin films, photocatalytic properties are primarily affected by surface recombination. An efficient minimization of such mechanism necessitates crystals large enough. For too small crystals, surface recombination competes with intergranular charge transfer and inhibits migration of charge carrier from deeper layers toward film surface. On the other hand, as indicated in introduction, too large crystals induce an enhanced contribution of the volume recombination, which then reduces the photocatalytic activity. The fact that the photoactivity does not increase when increasing the annealing temperature above 600°C (Fig. 14) might thus attributed to an excessive crystal size (around 60 nm for MS films annealed at 700°C).

3.5.4. Normalized photoactivity of CS films

The temperature dependence of the normalized activity of CS/90/130 films is illustrated in Fig. 15. As already illustrated in Fig. 13, owing to their rather good crystallization degree, as-deposited CS/90/130 films exhibit a significant photoactivity. However, their normalized activity is about 40% lower than that measured on best MS films annealed at 600°C, which is presumably related to amorphous matter remaining at grain boundaries. Fig. 15 shows that the photoactivity of CS/90/130 films weakly decreases for annealing temperature increasing up to 400°C. Since these photoactivity variations are close to the experimental error, they should not be further discussed here. However, let us recall that in this low temperature range, CS films did not undergo marked densification and structural modifications. The photoactivity of CS/90/130 films significantly decreases when increasing temperature from 500 to 700°C, despite a marked increase of their densification and crystallization degrees. This activity decrease suggests in particular that, contrary to MS films, the photoactivity of anatase CS films would continuously decrease with increasing crystal size. For instance, the photoactivity of a CS/90/130 film annealed at 700°C was three times weaker than that measured for a MS film annealed at 600°C, despite a comparable crystal size (50 nm) and similar densification and crystallization degrees. Fig. 15 also shows that the rutile CS/90/130 film annealed at 800°C, exhibits almost no activity. This presumably illustrates the very poor activity of the rutile phase together with a possible effect of the large size of crystallites constituting this film (140 nm).

The fact that CS films are composed of aggregated crystallites might account for differences observed in photocatalytic activities of MS (Fig. 14) and CS/90/130 films (Fig. 15). Because thermal densification of CS films, which occurs above 400°C, essentially takes place within aggregates, intergranular transfer within aggregates would be enhanced with increasing temperature. Denser aggregates might thus more or less behave like large single crystals (around 100 nm in size, according to SEM observations), where volume recombination of charge carriers would predominate. Volume recombination would in turn reduce the flux of charge carriers reaching the film surface in contact with matter to be decomposed. In other words, in the case of aggregated CS films, the

photoactivity would be governed by aggregate rather than crystal size. This implies in turn that, in the case of aggregated films, while a too great porosity inhibits intergranular charge transfer, a sufficient porosity might be required for regulating the charge carrier flux within aggregate, thus preventing a fast volume recombination. There should therefore exist an optimum in terms of intra-aggregate porosity. This conclusion can in turn presumably be extrapolated to the whole film thickness. For a given grain (crystallite or aggregate) size, an optimum of intergranular porosity should exist, which should be compatible with an efficient intergranular charge carrier transfer and should allow preventing too fast charge carrier recombination within film thickness. Fig. 13 shows that CS/90/130 films with a porosity of 30 vol% have a greater photoactivity than CS/30/200 films with a porosity of 40 vol%. Besides, Fig. 15 shows that the photoactivity of CS/90/130 films with a porosity of 30 vol% have a greater photoactivity than CS/30/200 films with a porosity of 40 vol%. Besides, Fig. 15 shows that the photoactivity of CS/90/130 films decreases when increasing the annealing temperature above 500°C. In the same time, the film porosity decreases below 30 vol%. These results suggest that for CS films, a porosity around 30 vol% might be an optimum value. On the other hand, the maximum photoactivity reached after annealing MS films at 600°C (Fig. 14) might not only rely on a crystal size optimum, but also on a porosity optimum, which would correspond to a value of 15 vol%. This optimum value is significantly weaker than for CS films because aggregated or nonaggregated morphologies of CS and MS films influence differently the charge carrier transfer. It is likely that other physico-structural parameters can also contribute to difference observed in the photocatalytic properties of CS and MS films. For instance, it is not excluded that the partial [001] orientation evidenced for MS films plays a role in their photoactivity.

3.5.5. Normalized photoactivity of CS/10/200 films

As mentioned in Sections 3.1 to 3.4, CS/10/200 films exhibit very specific physico-structural properties when compared to other CS films. A special attention was therefore paid to their photocatalytic properties. Fig. 16 shows that the photoactivity of CS/10/200 films follows a bi-regime behavior. In a first regime, this photoactivity slightly increases with increasing temperature up to 500°C. At this temperature, the photoactivity of a CS/10/200 film is about 50% greater than that of a CS/90/130 film. CS/10/200 films annealed at higher temperature undergo photoactivity variations similar to that of CS/90/130 films, i.e. a marked undergo photoactivity decrease with increasing temperature. But for a same temperature photoactivities of the former remain greater than that of the latter. Ellipsometric and SEM measurements have shown that CS/10/200 films are much more porous

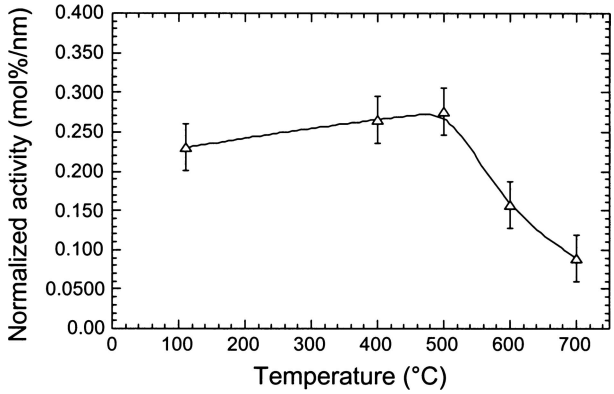

Figure 16 Normalized photoactivity versus annealing temperature for CS/10/200 films. The photoactivity has been normalized with respect to the effective film thickness t_o. Lines are drawn only to guide the eye.

than CS/90/130 films, with a porosity ranging from c.a. 40 to 50 vol%, which depends on the annealing temperature. The greater photoactivity of CS/10/200 films might therefore appear to be in apparent contradiction with previous features showing that, for CS/90/130 films a 30 vol% porosity seems to be an optimum value. However, let us recall that CS/10/200 films exhibit a very particular morphology, with large pore sizes that were not observed for any other CS films. It is therefore likely that, in this case, liquid reactant is able to impregnate large pores yielding an enhanced contact surface with photocatalytic particles. This enhanced contact surface might partially compensate for the effects of charge carrier recombination within large aggregates, leading to a greater photoactivity. The bi-regime behavior illustrated in Fig. 16 might therefore traduce a competitive mechanism between charge carrier transfer through the film thikness and film impregnation by the liquid reactant. A first regime would be governed by an enhancement of the crystallization degree at the grain surface, which would favour a better intra-aggregate charge transfer toward the impregnated liquid. A higher temperature second regime would be governed by intra-aggregate densification, which would promote a faster recombination of charge carriers within the volume of densified aggregates.

Two additional features can account for differences in the photoactivities of CS/10/200 and other CS films. Quantization effects might ensue from the small crystal size (6 nm) measured for CS/90/130 or CS/200/100 films annealed below 400°C. A larger band gap induced by quantization effects might reduced UV absorption in our irradiation conditions ($\lambda > 340$ nm). Such a feature would not be observed in CS/10/200 films annealed in the same temperature range, owing to a larger crystal size of 10 nm. However, according to a theoretical prediction proposed by Brus [33], we have calculated that a 6 nm diameter would induce a 0.02 eV ($\Delta\lambda = 2.4$ nm) blue shift from the bulk-phase band gap for anatase (3.2 eV), which is extremely weak. Accordingly, all as-deposited CS films exhibited comparable band edge absorption in the near-UV range (not shown here). This seems to indicate that

eventual quantization effects should remain rather weak in CS films. On the other hand, the particular morphology of CS/10/200 films could influence the interaction of UV radiation with photocatalytic particles. In particular, owing to a greater porosity, these films exhibit a weaker refractive index, which reduce reflections at the film surface. This might promote a more efficient penetration of UV radiation within the film, leading to enhanced photoactivities. In any cases, further studies are required to better understand photocatalytic properties of MS and CS films.

4. Conclusion

Sol-gel derived photocatalytic TiO_2 films were deposited from different MS and CS sols and annealed at various temperatures. Upon annealing, CS films undergo a crystal growth that is controlled by grain boundary diffusion mechanism, while MS films undergo a nucleation/growth mechanism within the as-deposited amorphous medium. Depending on sol formulations and annealing temperatures, a large range of crystal sizes could be controlled. Results show that sol formulations and annealing temperatures also influence densification and crystallization degrees of the films, as well as their surface morphologies. The film photoactivity shows a complex dependence on the different physico-structural parameters. For films with a large pore size, liquid reactant to be photocatalytically decomposed is able to penetrate pores, which induces a better catalyst/reactant contact surface and favors a greater photoactivity. In the more general case of films with fine porosity, the photoactivity is governed by migration of charge carriers from deeper layers toward surface of the film. This charge carrier transfer is affected by recombination mechanisms at the surface or within the volume of grains (crystals or aggregates). An efficient charge carrier transfer through the film thickness requires optimum grain size and film porosity. A maximum photoactivity was measured on rather dense and non-aggregated MS films with a crystal size around 50 nm. This size appears to be an ideal compromise, which allows minimizing both surface and volume recombination mechanisms.

Acknowledgments

The authors wish to thank J.M. Herrmann, C. Guillard, and P. Pichat, for their help in photocatalytic measurements.

References

1. M. ANPO, T. SHIMA, S. KODAMA and Y. KUBOKAWA, *J. Phys. Chem.* **91** (1987) 4305.
2. W. CHOI, A. TERMIN and M. R. HOFFMAN, *ibid.* **98** (1994) 13669.
3. J. M. NEDELJKOVIC, M. T. NENADOVIC, O. I. MICIC and A. J. NOZIK, *ibid.* **90** (1986) 12.
4. Z. ZHANG, C. C. WANG, R. ZAKARIA and J. Y. YING, *J. Phys. Chem B* **102** (1998) 10871.
5. A. J. MAIRA, K. L. YEUNG, C. Y. LEE, P. L. YUE and C. K. CHAN, *J. Catalysis* **192** (2000) 185.
6. S. ITO, S. INOUE, H. KAWADA, M. HARA, M. IWASAKI and H. TADA, *J. Colloid Interface Sci.* **216** (1999) 59.
7. J. F. PORTER, Y. G. LI and K. C. K. CHAN, *J. Mater. Sci.* **34** (1999) 1523.
8. C. H. CHO and D. K. KIM, *J. Am. Ceram. Soc.* **86**(7) (2003) 1138.
9. A. H. C. CHAN, J. F. PORTER, J. P. BARFORD and C. K. CHAN, *J. Mater. Res.* **17**(7) (2002) 1758.
10. J. C. YU, W. HO, J. LIN, H. YIP and P. K. WONG, *Environ. Sci. Tech.* **37** (2003) 2296.
11. A. MILLS, A. LEPRE, N. ELLIOTT, S. BHOPAL, I. P. PARKIN and S. A. O'NEILL, *J. Photochem. Photobiol. A: Chem.* **160** (2003) 213.
12. M. LANGLET, A. KIM, M. AUDIER, C. GUILLARD and J. M. HERRMANN, *J. Mater. Sci.* **38** (2003) 3945.
13. M. BORN and E. WOLF, "Principle of Optics" (Pergamon, New York 1975) p. 85.
14. J. M. HERRMANN, *Catalysis Today* **53** (1999) 115.
15. M. LANGLET, A. KIM, M. AUDIER and J. M. HERRMANN, *J. Sol-Gel Sci. Tech.* **25** (2002) 223.
16. M. BURGOS and M. LANGLET, *Thin Solid Films* **349** (1999) 19.
17. R. J. GONZALES, R. ZALLEN and H. BERGER, *Phys. Rev. B* **55**(11) (1997) 7014.
18. G. BUSCA, G. RAMIS, J. M. GALLARDO AMORES, V. SANCHEZ ESCRIBANO and P. PIAGGIO, *J. Chem. Soc. Faraday Trans.* **90**(20) (1994) 3181.
19. M. OCANA, V. FORNES, J. V. GARCIA RAMOS and C. J. SERNA, *J. Sol. State Chem.* **75** (1988) 364.
20. M. OCANA and C. J. SERNA, *Spectrochim. Acta* **47A** (1991) 765.
21. C. PECHARROMAN, F. GRACIA, J. P. HOLGADO, M. OCANA, A. R. GONZALES-ELIPE, J. BASSAS, J. SANTISO and A. FIGUERAS, *J. Appl. Phys.* **93**(8) (2003) 4634.
22. C. J. BRINKER and G. W. SCHERER, "Sol-Gel Science, The Physics and Chemistry of Sol-Gel Processing" (Academic Press, San Diego, 1990), p. 675.
23. "Handbook of Chemistry and Physics" (The Chemical Rubber Co., Cleveland Ohio, 1967), 48th edn. B-279.
24. G. BALDINOZZI, D. SIMEONE, D. GOSSET and M. DUTHEIL, *Phys. Rev. Lett.* **90**(21) (2003) 216101.
25. K.-N. P. KUMAR, K. KEIZER, A. J. BURGRAAF, T. OKUBO, H. NAGAMOTO and S. MOROOKA, *Nature* **358** (1992) 48.
26. K-N. P. KUMAR, J. KUMAR and K. KEIZER, *J. Am. Ceram. Soc.* **77**(5) (1994) 1396.
27. R. R. BACSA and M. GRÄTZEL, *ibid.* **79**(8) (1996) 2185.
28. B. L. BISCHOFF and M. A. ANDERSON, *Chem. Mater.* **7** (1995) 1772.
29. Y. OGURI, R. E. RIMAN and H. K. BOWEN, *J. Mater. Sci.* **23** (1988) 2897.
30. A. CHEMSEDDINE and T. MORITZ, *Eur. J. Inorg. Chem.* (1999) 235.
31. K. TERABE, K. KATO, H. MIYAZAKI, S. YAMAGUCHI, A. IMAI and Y. IGUCHI, *J. Mater. Sci.* **29** (1994) 1617.
32. S. MUSIC, M. GOTIC, M. IVANDA, S. POPOVIC, A. TURKOVIC, R. TROJKO, A. SEKULIC and K. FURIC, *Mater. Sci. Eng.* **B47** (1997) 33.
33. L. BRUS, *J. Phys. Chem.* **90** (1986) 2555.

Received 13 August 2004
and accepted 22 June 2005